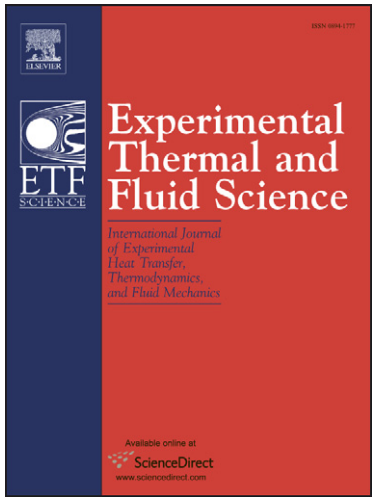

Electric field effects during nucleate boiling from an artificial nucleation site

S. Siedel, S. Cioulachtjian, A.J. Robinson, J. Bonjour

PII: S0894-1777(10)00118-4
DOI: 10.1016/j.expthermflusci.2010.06.006
Reference: ETF 7356

To appear in: *Experimental Thermal and Fluid Science*

Received Date: 2 February 2010
Revised Date: 4 June 2010
Accepted Date: 15 June 2010

Please cite this article as: S. Siedel, S. Cioulachtjian, A.J. Robinson, J. Bonjour, Electric field effects during nucleate boiling from an artificial nucleation site, *Experimental Thermal and Fluid Science* (2010), doi: 10.1016/j.expthermflusci.2010.06.006

Electric field effects during nucleate boiling from an artificial nucleation site

S. Siedel[a,b,1], S. Cioulachtjian[a,2], A.J. Robinson[b,3], J. Bonjour[a,4]

[a] Université de Lyon, CNRS

INSA-Lyon, CETHIL, UMR5008, F-69621, Villeurbanne, France

Université Lyon 1, F-69622, France

[b] Department of Mechanical and Manufacturing Engineering, Parsons Building, Trinity College Dublin, Ireland

[1] Email: samuel.siedel@insa-lyon.fr

[2] Email: serge.cioulachtjian@insa-lyon.fr

[3] Tel: +343 (0)1.896.3919, Email: arobins@tcd.ie

[4] corresponding author: Tel: +33 (0)4.72.43.64.27, Fax: +33 (0)4.72.43.88.11, Email: jocelyn.bonjour@insa-lyon.fr

Abstract

An experimental study of saturated pool boiling from a single artificial nucleation site on a polished copper surface has been performed. Isolated bubbles grow and depart from the artificial cavity and the bubble dynamics are recorded with a high speed camera. Experimental results are obtained for bubble growth, departure and vertical rise both with and without the application of an electric field between an upper electrode and the boiling surface. As detailed in a previous paper from the same research group the high spatial and temporal resolution of the video sequences facilitated the development of a baseline experimental bubble growth law which predicts the bubble volumetric growth characteristics for a range of surface superheats at atmospheric pressure. The presence of an electric field has been found to positively augment the convective heat transfer over that of buoyant natural convection. Further to this, for high electric field strengths, the bubble shape,

volumetric growth characteristics and bubble rise are different from that of the baseline cases. These results provide compelling evidence that electric fields can be implemented to alter the bubble dynamics and subsequent heat transfer rates during boiling of dielectric liquids.

1 Introduction

Pool boiling heat transfer is characterized by very high dissipated heat fluxes whilst requiring low driving temperature differences. In the nucleate pool boiling regime the high heat transfer rates are primarily due to enhanced convection, transient conduction, microlayer evaporation, and contact line heat transfer brought about by the motion of the bubbles [1]. The relative contribution of each individual heat transfer mechanism to the overall heat transfer rate is sensitive to the boiling condition and difficult to predict. What is obvious is that the boiling heat transfer coefficient is intimately linked to the bubble dynamics: that roughly being bubble nucleation, growth, and detachment, as well as factors such as nucleation site density and interactions between neighbouring and successive bubbles [2]. Therefore, in order to gain insight into the heat transfer mechanisms during boiling a fundamental understanding of the bubble dynamics is required.

Since boiling heat transfer affords a very effective means to transfer heat, it is implemented in numerous technologies and industries ranging from large power generation plants to microelectronics thermal management. No matter what the scale of the technology, industries are continually demanding smarter and smaller heat exchangers. A promising technique for improving and controlling the heat transfer during boiling is the introduction of an electric field. This technique is generally termed electrohydrodynamics (EHD). Whether for pool boiling or convective boiling

scenarios, several studies have shown that EHD can considerably augment two phase heat transfer [3-8].

Previous research on EHD augmentation of boiling and condensation has shown that the electrical influences on two-phase systems are due to the addition of electrical body forces. As detailed in Panofsky and Phillips [9] and Chang and Watson [10], these electric forces can be represented by the expression:

$$\vec{F_E} = \rho_{el}\vec{E} - \frac{1}{2}\vec{E}^2\vec{\nabla}\epsilon + \frac{1}{2}\vec{\nabla}\left[\rho\vec{E}^2\left(\frac{\partial\epsilon}{\partial\rho}\right)_T\right] \quad (1)$$

The three terms on the right-hand side of Eq. (1) represent the *electrophoretic, dielectrophoretic,* and *electrostrictive* components of the force, respectively. The electrophoretic force results from the net free charge within the fluid or injected from the electrodes and is the only force which depends on the direction of the electric field. The dielectrophoretic force is a consequence of inhomogeneity or spatial change in the permittivity of the dielectric fluid due to non-uniform electric fields, temperature gradients, and phase discontinuities. The electrostrictive force is caused by inhomogeneous electric field strength and the variation in dielectric constant with temperature and density.

For isolated bubbles growing either by vaporization or by gas injection, previous research has found that the electric field tends to elongate the bubble in the direction of the electric field due to non-uniformity of the electrically induced stresses on the bubble surface [11-13]. Generally, the degree of elongation or deformation tends to increase with the electric field strength [12]. Bubble detachment sizes and growth periods are also affected by the presence of an electric field, though there is not at the moment a clear consensus as to the fundamental mechanisms which in some cases cause them to increase and in others decrease. For surface boiling with a

large number of nucleation sites on a natural surface, Kweon and Kim [14] observed smaller detachment sizes. This is also generally the case for isolated bubbles growing in non-uniform electric fields [8, 15]. However, for single bubble events in axisymmetric or uniform electric fields, the detachment volume of the bubble has been observed to in some cases increase, decrease or remains unchanged [11, 12, 15].

With regard to the heat transfer, Liu et al. [8] recently utilized a microheater array held at constant temperature to measure the surface heat flux beneath the heater for both an upward and downward facing surface in a non-uniform electric field. For the upward facing tests, a moderate heat transfer enhancement was measured with more rapid bubble nucleation and growth and more frequent detachment compared with the field-free case. For the downward facing surface, bubbles detached regularly in the presence of an electric field whereas no bubble detachment was observed without the aid of an electric field. In this configuration a significant heat transfer enhancement was measured when the electric field was applied.

It is clear that there is sufficient evidence in the open literature to indicate that the bubble dynamics and boiling heat transfer are strongly influenced by the presence of an electric field. It is also clear that the number of parameters which influence the phenomenon are extensive enough that there exists inconsistencies and contradictions in the observed phenomena. Advanced numerical investigations, such as those by Zu and Yan [16] or Zhang et al. [17], as well as more fundamental experimental studies on the influence of EHD on boiling dynamics, are required to progress this area of thermal science.

In order to provide further insight into the influence of EHD on single bubble events during boiling, a simple experiment has been devised which involves as few variables

as possible whilst providing bubble growth measurements with high spatial and temporal resolution. Importantly, bubble growth data for the field-free cases from Siedel et al. [18] have provided the reliable baseline growth data to which the EHD cases have been compared and contrasted in order to gain further physical insight into this phenomenon.

2 Experimental setup and procedure

2.1 Boiling vessel

The experimental apparatus, shown schematically in Fig. 1, consists of a sealed 250 mm x 250 mm x 180 mm vessel. To facilitate observation and photography within the vessel the vertical faces of the vessel were equipped with rectangular windows which were sealed to the main housing of the tank.

Initially the tank was evacuated and subsequently filled with 99% pure n-pentane. The free surface between the liquid and vapour phases was at a height of approximately 220 mm from the base of the container. N-pentane was chosen as the working fluid as it has desirable properties; in particular it is non-toxic, non-polar, has a relatively low boiling point (35.7℃) and has a liquid permittivity approximately twice that of the vapour phase.

A 350 W cartridge heater was immersed in the liquid pentane. Initially, this heater was utilized to over-pressurize the vessel to facilitate purging of dissolved gasses. Subsequent to this degassing stage, the immersion heater was implemented to control the saturation temperature and pressure of the working fluid during testing. Four thermocouples were placed close to the test sample, in the vapour phase and in the upper and lower part of the liquid phase to monitor and control the saturation condition as well as to ensure temperature homogeneity within and between the liquid and vapour phases.

2.2 Heater surface and electric field generation

Boiling took place atop the metered heater element illustrated in Fig. 2. The heater element was situated in the centre of the vessel with the upper surface nominally 100 mm below the vapour-liquid free surface of the n-pentane, as depicted in Fig. 1.

The heater element was constructed from a 12 mm diameter solid copper cylinder. The lower end was machined to receive a 50 mm long 300 W cartridge heater with a diameter of 8 mm. In order to increase the axial heat flux as well as reduce the overall area of heat transfer at the exposed end of the heater element, the upper portion of the copper rod was reduced to a diameter of 5 mm. The upper portion of the copper pin section was equipped with six K-type thermocouples to monitor the axial temperature distribution. The entire heater element except the top surface was encased in PTFE in order to provide sufficient insulation to reduce radial heat losses.

The boiling surface consisted of a 40 μm thin and 18 mm diameter copper sheet which was soldered to the top surface of the copper pin section. The plate was mirror-polished to reduce the number of potential nucleation sites on its surface. The plate was also thin enough to restrict radial heat flow to the extent that nucleation, and thus boiling, was avoided at its outer edge during tests.

A single artificial nucleation site was created by mechanical indentation at the centre of the plate. A tungsten carbide needle was constructed in-house and was positioned to be in intimate contact with the surface. It was then forced into the surface with its displacements accurately measured during the entire indentation process. The surface geometry of the site has been measured with a confocal white light microscope. As shown in Fig. 3, the 500 μm deep cavity is generally parabolic and has a diameter of 180 μm. Approximately 20K to 30K of superheat was required to initiate boiling at the artificial nucleation site. As a result of the care taken in the

surface preparation and cleaning, boiling only occurred at this artificial nucleation site. At such high wall superheats, the nucleation site produces bubbles at such a rate as to generate a nearly continuous vapour column. As this boiling regime was not the focus of this investigation, the heat flux was reduced to the extent that the wall superheat was maintained between 1.5 and 8 K. This superheat range was high enough to generate discrete bubble events, albeit with very small waiting times, whilst being high enough to keep the nucleation site active.

In order to generate a strong DC electric field in the vicinity of the boiling surface, a brass screen mesh electrode was fixed approximately 7 mm above the boiling surface and arranged parallel to the surface, as depicted in Fig. 1. The electric field within the working fluid was generated by placing a voltage potential between the electrode and the boiling surface which was connected to ground with a HEINZINGER PNC 30000 high voltage power supply capable of producing between 0 to 30 kV.

2.3 Photography and image processing

As mentioned, boiling only took place in the middle of the vessel occurring at the centre of the copper boiling surface. As will be discussed, subsequent to detachment the bubbles rose more or less vertically in the bulk liquid, passing through the wire mesh upper electrode and onward to the free surface. In order to capture the bubble growth, departure and rise dynamics with high enough temporal and spatial resolution, a Photron Fastcam 1024 PCI high speed digital camera was utilised. The bubble was illuminated with a diffuse backlight at a frequency of 200 kHz. The camera was capable of recording the bubble growth and rise over a vertical span of 12 mm at image acquisition frequencies in the range of 1000 to 3000 fps.

An in-house image processing code has been developed using the commercial Matlab software platform. Using the visual toolbox afforded by Matlab, the instantaneous bubble contour is detected by locating the maximum grey gradient using the Sobel method. A sample of the image processing sequence from the raw digital image to the reconstructed bubble interface is shown in Fig. 4. Subsequent to the bubble interface reconstruction the bubble volume is calculated by assuming axisymmetry and revolving each one pixel thick section around the vertical axis and summing each section volume from the tip to the base of the bubble. To calculate the location of the centre of gravity of the bubble, the vapour pressure within the bubble was assumed to be homogeneous and constant such that the vapour density can be approximated from available property data.

2.4 Data reduction and experimental uncertainty

The heat flux across a section of the copper rod was assumed to be uniform and was calculated with the expression,

$$q'' = -k_{Cu} \left. \frac{dT}{dz} \right|_{z_W} \tag{2}$$

where k_{Cu} is the thermal conductivity of the copper which was evaluated at the average block temperature and $dT/dz|_{z_W}$ is the magnitude of the slope of the polynomial regression fit to the six temperature measurements in the proximity of the upper surface. The estimation of the temperature gradient at the upper surface also facilitated the determination of the surface temperature, T_W, which is required for the determination of the wall superheat, given as,

$$\Theta_W = T_W - T_{sat}(P_\infty) \tag{3}$$

The surface temperature was determined by extrapolation of the temperature distribution to the surface:

$$T_w = T_1 + (z_w - z_1)\left(\left.\frac{dT}{dz}\right|_{z_w}\right) \quad (4)$$

where $z_w - z_1$ is the distance from the surface to the location of the thermocouple closest to the surface. The absolute uncertainties on the temperature measurement were estimated to be ± 0.1 K. An improved uncertainty of ± 0.05 K for the temperature differences between the thermocouples within the test sample was made possible by ensuring that the exact same thermocouple wire was used for each sensor. A 2D Monte-Carlo method described by Kempers et al. [18] was used to estimate the heat flux and surface temperature uncertainties with a 95 % confidence interval. The temperature values were considered as being distributed normally within their uncertainty band, while the thermocouple locations were considered as being distributed uniformly within a ±0.5 mm interval. The surface temperature uncertainty was ±0.15 K, leading to a 0.18 K uncertainty for the wall superheat.

The heat flux uncertainty was 47 % for low heat flux and reduced to 15 % for high heat flux levels. Included in this uncertainty is the additional error associated with the thermal conductivity of copper. This error had negligible influence on the temperature computations and is an offset error so that it is the same for each heat flux computation and does not influence the differences in the observed trends. i.e. it is not a random error. As no detailed quantitative analysis is performed on the heat flux, in the sense that only the relative trends are considered in Fig. 6, this error was viewed as acceptable.

3 Results and discussion

3.1 Single phase convection

The application of an electric field can affect the flow structure of a single phase system due to the electrically induced forces acting on the fluid particles. Evidence of this is clearly shown in Fig. 5 which are visualizations of the flow structure obtained with backward light and, for illustration purposes, at a rather extreme wall superheat of 30 K. In Fig. 5a, buoyant natural convection is occurring in which a large convective plume rises from the heater surface with fluid velocities in the approximate range of 5 to 10 mm/s. Upon application of an electric field, the flow structure is altered considerably, as depicted in Fig. 5b for an applied voltage of 24 kV. With an electric field, the plume originally observed above the boiling surface can no longer be observed. In its place, smaller convection cells appear in the entire field of view though tend to be concentrated within a few millimetres above the heated surface. Figure 6 shows the heat transfer characteristics for the current experimental setup for applied voltages in the range of 0-24 kV and heat fluxes in the range of 2000-12,000 W/m^2. The reference diameter for the heat flux is taken as 5 mm such that the heat flux is that along the top pin portion of the copper rod. It is evident that the application of the electric field enhances the heat transfer and that the enhancement tends to improve with increasing applied voltage.

Figure 6 includes an imbedded figure which quantifies the level of enhancement as the ratio of the heat flux with EHD to that without EHD for the highest applied voltage i.e. $q''_{24\ kV}/ q''_{0\ kV}$. In the lower wall superheat range the enhancement can be as high as 1.6 fold. This decreases with increasing heater temperature and tends towards unity. This is as one would expect since buoyancy forces become stronger at the higher superheats and should begin to dominate over the electrically induced forces.

3.2 Bubble growth and detachment with and without an electric field

In a previous study [19], field-free bubble growth measurements were performed for a superheat range of $2.1 \leq \theta_w \leq 7.1$K. It is worth noting that these boiling tests can be considered to be at quite low Jakob numbers, being in the range of $2.7 \leq Ja \leq 10.5$. Here the Jakob number is calculated based on the wall superheat such that,

$$Ja = \frac{\rho_l C_p \Theta_w}{\rho_v h_{fg}} \tag{5}$$

Robinson and Judd [20] proposed an order of magnitude criterion which should indicate whether bubble growth would be expected to be diffusion controlled or whether inertial influenced, associated with the kinetic energy of the surrounding liquid, would be the dominant influence. Based on a simple scaling argument the criterion was posed as,

$$I_R = \left(\frac{4}{27}\right)\left(\frac{\sigma}{\rho_l a^2}\right)\frac{R_c}{Ja^2} \quad \begin{cases} \ll 1: \text{Inertia controlled} \\ \gg 1: \text{Diffusion controlled} \end{cases} \tag{6}$$

where R_c is the bubble radius at nucleation, taken here as the cavity radius. For the Jakob number range of this study, I_R lies between 500 and 7700, which indicates that bubble growth is diffusion controlled and inertial influences are negligible.

With regard to the bubble growth regime, an analysis on the forces governing bubble detachment has been performed and is detailed in Appendix 1. The buoyancy and contact pressure forces are balanced by the surface tension forces at the triple contact line. Inertial forces are negligible close to detachment.

As depicted in Fig. 7a the bubbles that grew from the artificial nucleation site without an electric field were originally spherical in shape. Further, the bubble foot remained attached to the rim of the nucleation site during the entire growth period i.e. the triple contact line remained stationary. In the mid-growth stages the bubble shape began to

deviate from that of a spherical segment. Here, buoyancy is pulling the bubble away from the wall whilst the surface tension force is keeping the bubble foot attached to the wall. This causes the bubble base region to stretch and elongate whilst the bubble cap remains more or less spherical in shape. This action continues until buoyancy is sufficient to cause a neck to form. The neck soon pinches after which the bubble detaches and rises in the bulk liquid. Subsequent to bubble departure, the next bubble very quickly begins its growth resulting in an immeasurable waiting time. As has been reported in Siedel et al. [19], the bubble frequency was found to increase linearly with the wall superheat whereas the bubble volume at detachment was more or less independent of superheat and equal to 0.55 ± 0.02 mm^3.

Fig. 7b shows the bubble growth sequence photographically for a similar wall superheat though with 24 kV applied between the electrode and the heater surface. It is immediately apparent that the electrically induced stresses on the bubble surface have a profound effect on the bubble shape and subsequent growth dynamics. Even at the earliest stage of growth the bubble tends to elongate compared with the field-free case. The bubble distortion becomes more pronounced as the bubble gets larger. Even though the growth dynamics have been altered considerably, the growth time and departure diameters were not altered significantly compared with the field-free tests, generally being within ± 10 %.

Bubble growth dynamics are governed by the complicated interaction of the flow and thermal field with the bubble itself. It is common to characterize bubble growth in terms of an equivalent radius, often calculated from the measured volume [11, 22]. However, bubbles growing from a nucleation site or submerged orifice are only spherical segments during the initial phase of growth. Since the bubble shape is generally not that of a spherical segment, a more appropriate parameter to gauge the

bubble size is its volume. This is a particularly relevant approach during boiling with EHD since the bubble shape is often very far from spherical.

Figure 8 gives the bubble volumetric growth curves for various superheats for the field-free cases. Here, the bubble growth curves have been made non-dimensional by normalizing the time by the total growth time and the volume by the departure volume. It is clear that the field-free growth curves collapse very well onto a single curve showing that the non-dimensional growth is independent of wall superheat for the range of Jakob numbers tested. The best fit curves shown in Fig. 9 were made by fitting several independent bubble growth histories for 16 different superheats. As reported in [19], the non-dimensional growth is well described by two distinct asymptotes, one for early growth and one for mid and late growth;

$$V' = \begin{cases} 2 \times t' & \text{for } t' < 0.2 \\ t'^{0.6} & \text{for } t' > 0.2 \end{cases} \quad (7)$$

Since inertial forces are negligibly small, the difference in the functional relationship between early growth and mid to late growth must be a consequence of a difference in the heat transfer characteristics.

The functional relationship of this empirical growth law is notably different from classical growth laws which are typically asymptotic and of the form $R = Ct^{0.5}$. This would result in a volume growth relationship of the form $V' = t'^{1.5}$, which is clearly not the case in this study. An energy balance, considering the bubble as a control volume, relates the latent heat transported into the bubble to the overall heat transfer into the bubble by conduction within the liquid phase and, for a constant vapour density, can be expressed as,

$$\rho_v h_{fg} \frac{dV}{dt} = \int_A k \frac{\partial T}{\partial n} dA \quad (8)$$

where A is the instantaneous bubble surface area and $\partial T/\partial n$ is the local temperature gradient normal to the interface. Thus, the rate of change of the bubble volume is an important parameter in the sense that it provides rich information regarding the time history of the rate of energy transfer into the bubble. For instances in which $V \propto t^n$ and n > 1, this implies that the rate of change of the volume, and thus the rate of energy transfer, continually increases. However, once a bubble nucleates it continually depletes the sensible energy stored within the liquid surrounding it. Thus, for the rate of energy transfer to increase, it must be that the volumetric growth rate is large enough that the surface area available for heat transfer increases at a rate which is more than sufficient to offset the fact that the local heat flux levels are decreasing. For the case here, where $V \propto t^n$ and n < 1, the rate of change of the volume and thus the rate of energy transfer continually decrease, as depicted in Fig. 10. Thus, for these low Jakob numbers, possibly in combination with the negligibly small waiting times, the volumetric growth rate is not sufficient to sustain vapour production as the energy in the surrounding liquid is depleted. During early growth, t' < 0.2, the relatively high rate of heat transfer/vapour generation is maintained with dV'/dt'~2. For t>0.2 it decreases steeply and begins to plateau to a near uniform value of dV'/dt'~0.6.

Fig. 9 shows the volumetric growth curves for the case of 24 kV applied voltage. Clearly, the electric field has a notable influence on the growth characteristics. For this applied voltage level the curvature of the growth curve is significantly reduced which is indicative of an increase in the exponent associated with the power law dependence. The curve is well correlated as,

$$V^{*} = \begin{cases} 1.2 \times t^{*} & \text{for} \quad t^{*} \leq 0.7 \\ t^{*0.45} & \text{for} \quad t^{*} > 0.7 \end{cases} \tag{9}$$

Considering the discussion above, the general increase in the magnitude of the exponent signifies a change in the rate of vapour production which is related to the flow and thermal field around the bubble as well as its size and shape. This is clearer in Fig. 10 where the rate of change of the non-dimensional bubble volume is plotted for the 24 kV case. Initially the vapour production rate is relatively uniform and lower than the field-free scenario. However, the level of vapour production is sustained for a large portion of the bubble lifetime though dipping in the final stage. The drastically different profiles depicted in Fig. 10 are evidence that the presence of the electric field has a very strong influence on the flow and thermal fields and how they interact with the growing bubble.

Even though it is clearly evident that the electric field influences the heat transfer, fluid mechanics and bubble properties, it will not be without more advanced CFD simulations that the mechanisms are understood with certainty and will be the subject of future work.

3.3 Bubble rise with and without an electric field

Immediately prior to bubble detachment a neck is formed between the base and cap of the bubble as shown previously in Fig. 7. Subsequent to its formation, the neck rapidly collapses, the free bubble oscillates slightly due to the neck breakage event and the bubble begins to float vertically upward with a near straight trajectory. At some point, the bubble deforms into an ellipsoid shape and soon afterwards changes trajectory and experiences a zigzag or spiral-type upward motion. A photographic sequence of a post departure bubble rise is given in Fig. 11 for a case without the application of an electric field.

For saturated boiling the volume of a bubble subsequent to departure should not change significantly. As the bubble breaks free from the surface it rises above the superheated boundary layer in the liquid immediately adjacent to the surface. Provided that most of the sensible energy within the relaxation macrolayer around the bubble dome had been depleted during the bubble growth phase, little phase change should occur as the bubble is in thermal equilibrium with its saturated surroundings. The short trajectory followed in the photographic sequences (12 mm) results in less than 0.3% variation of the hydrostatic pressure so that this will not compress the bubble enough to significantly reduce its volume. Thus, the apparent decrease in the bubble volume evident in Fig. 11 is the result of optical effects. Due to the narrow depth of field the rising bubble contour quickly becomes blurred if it moves slightly out of plane, and depending on the contrast settings of the image processing, the bubble volume may appear somewhat different even though it is actually invariant.

The instantaneous centre of gravity of the bubble has been calculated and its height is shown in Fig. 12 as a function of time. The measurements are regression fit with an appropriate polynomial function and the vertical velocity estimated by taking its derivative. The bubble vertical velocity calculations are given in Fig. 13. This figure indicates that the bubble initially accelerates and the rate of acceleration decreases with time/vertical displacement. This is due to the fact that the upwardly directed buoyancy force acting on the bubble exceeds the downwardly directed drag force and this difference diminishes as the rise velocity increases i.e. the drag force is proportional to the square of the bubble rise velocity. In certain scenarios the velocity would increase to such an extent that the drag force exactly balances the buoyancy force such that a constant terminal velocity is achieved. However, this is not the case for the bubbles in this investigation. As depicted in Fig. 13, the bubble accelerates in

the vertical direction until reaching a local maximum. Approaching the critical velocity, the bubble randomly changes direction. As depicted in Fig. 13, the horizontal position, *x,* remains the same during the acceleration phase and changes at the moment when the critical vertical velocity is reached. A similar behaviour was noted by Jenny et al. [23] for a free ascending sphere where the sudden change of direction would occur when an instability would disrupt the axisymmetry of the wake behind the sphere causing a plane oblique trajectory.

Bubble rise data has been collected for 20 different bubbles for different wall superheats between 1.5 and 8 K. The wall superheat has shown to have no significant influence on bubble rise characteristics. This owes to the fact that the departure volume is more or less constant for the range of parameters tested. In all cases, the bubble accelerates in a straight path until it reaches a maximum vertical velocity and randomly changes direction.

The mean bubble volume at detachment was found to be 0.55 mm^3 which can be assumed constant during the bubble rise as discussed above. The mean experimentally determined peak velocity is 331 mm/s with a standard deviation of 12 mm/s. This velocity has been compared with the Peebles and Garber [24] correlation given as,

$$v_{max} = 0.33 \times g^{0.76} \left(\frac{\rho_l}{\mu_l}\right)^{0.52} R_{eq}^{1.28} \tag{10}$$

$$\text{With} \quad 2 \leq Re \leq 4.02 \left(\frac{We^3}{Re^4 Fr}\right)^{-0.214} \tag{11}$$

The characteristic length used for the dimensionless numbers *Re*, *We* and *Fr* was chosen to be the equivalent radius of the bubble at departure. The maximum velocity calculated with this correlation is 299 mm/s with a Reynolds number of *Re* = 2.5. The

measured and predicted values are within 10% of each other which is a sufficiently small percentage difference to suggest that the bubble rise mechanisms are identical even though the Peebles and Garber correlation was developed for adiabatic bubble rise. This is not particularly surprising considering that the bubble rise velocity is an order of magnitude higher than the rise velocity of the convective plumes which would indicate that the inertial effects of the rising liquid due to buoyant natural convection would not be significant.

As previously mentioned, when a uniform DC electric field is applied above a heated surface the single-phase convective flow structure is modified considerably as depicted in Fig. 5. The electrically induced forces within the liquid phase cause small convection cells to appear near the heated surface. Also, the electrically induced stress field distorts and elongates bubbles growing at the artificial nucleation site as depicted in Fig. 7. Even still, there is no significant change in the departure volume. This being the case, the bubble rise behaviour in the presence of an electric field generally tends to be similar to that of the no electric field cases. The mean peak velocity has been computed for numerous bubbles at various electric field intensities for both positive and negative polarities and the results are plotted in Fig. 14. In the figure the uncertainty bars correspond with one standard deviation from the mean maximum velocity.

It is evident that the peak vertical velocity of the bubbles decreases with increasing electric field intensity and the effect is more prominent with negative polarity. The fact that the same general trend is observed for both polarities suggests that the dielectrophoretic component of the force is likely responsible since it is independent of polarity. For the negative polarity cases it seems that the dielectrophoretic force

and the electrophoretic force tend to act together causing the drop in the peak velocity to be more pronounced.

Conclusion

Bubble growth measurements have been obtained for low Jakob number boiling at an artificial nucleation site. The growth, departure and rise of single bubbles have been recorded with a high speed camera both with and without the application of an electric field. The field-free baseline volumetric growth curves collapse onto a single curve when made non-dimensional by the departure volume and growth time. The universal curve is initially linear and becomes asymptotic for mid to late growth. The change in the functional relationship indicates a change in the bubble growth mechanisms which has been discounted as inertial influences. Subsequent to bubble departure the free bubble rises in the bulk liquid in a straight path until a peak velocity is reached. After this point the bubble follows a zigzag or spiral type of trajectory.

An electric field augments both the single phase convective heat transfer as well as the bubble growth and rise dynamics. During the growth stage the bubbles are elongated due to the electrically induced stresses acting on the bubble interface. The growth characteristics are notably different compared with that of the field-free baseline cases. The measurements indicate that the rate of heat transfer/vapour generation is initially lower than the field-free cases though tends to be sustained for a large portion of the bubble lifetime. Compared with the cases with EHD, for the field-free case the vapour generation rate is initially almost twice as high though drops off quite early in the bubble life.

Bubble rise has also been found to be influenced by the presence of an electric field. In particular, the peak velocity tends to decrease with electric field strength regardless of polarity, suggesting that this is the dielectrophoretic force. Even still, the

suppressing influence seems to be more pronounced for negative polarities indicating that two or more influences may be acting together though this hypothesis needs to be substantiated, possibly with more in-depth numerical simulations.,

Acknowledgment

This work was prepared in the frame of the CNRS thematic network GDR3057 "Analyse, Maîtrise des Ecoulements et Echanges Thermiques", AMETh.

Financial help for the academic visit of A.J. Robinson to CETHIL in 2010 from INSA is gratefully acknowledged.

Nomenclature

A	Area [m^2]
C_p	Specific heat capacity of the liquid phase [J/kg.K]
C_s	Constant in the unsteady growth force formulation []
d_w	Bubble contact diameter [m]
E	Electric field intensity [V/m]
f	Bubble frequency [Hz]
F	Force [N]
Fr	Froude number (= v^2 / gL) [-]
g	Gravitational acceleration [m^2/s]
h	Height of the centre of gravity of the bubble in the vertical direction [m]
h_{fg}	Latent heat of vaporization [J/kg]
I_R	Inertial growth criterion (= (4 / 27)(σ / $\rho_l\alpha^2$)(R_C / Ja^2)) [-]
Ja	Jacob number (= $\rho_l C_p \theta_W$ / $\rho_v h_{fg}$) [-]
k	Thermal conductivity [W/m·K]
L	Length [m]

P_∞ Pressure of the bulk liquid [Pa]

q Heat flux [W/m^2]

r_r Radius of curvature at the base of the bubble [m]

R Equivalent radius of the bubble (i.e. radius of a sphere that has the same volume) or radius of a spherical bubble [m]

R_C Nucleation radius of the bubble [m]

Re Reynolds number (= $\rho_l v L / \mu$) [-]

t Time [s]

t' Non dimensional time (i.e. time / total bubble growth time) [-]

T Temperature [K]

v Velocity [m/s]

v_{max} Bubble maximum vertical velocity [m/s]

V Bubble volume [m^3]

V' Non dimensional volume (i.e. bubble volume / bubble volume at detachment) [-]

V_0 Voltage between the electrodes [V]

We Weber number (= $2Lv^2\rho_l / \sigma$) [-]

x Bubble horizontal position [m]

z Position on the vertical axis of the experimental vessel [m]

Greek symbols

α Thermal diffusivity [m^2/s]

ε Relative dielectric permittivity of the fluid [-]

Γ Contact angle [rad]

μ Dynamic viscosity [Pa·s]

ρ	Density [kg/m^3]
ρ_{ei}	Density of electric charges [C/m^3]
θ_W	Wall superheat [K]
σ	Surface tension [N/m]

Subscripts

buy	Buoyancy
cp	Contact pressure
Cu	Copper
d	detachment
E	Electric
l	Liquid phase
sat	Saturation condition
ug	Unsteady growth
v	Vapour phase
w	Wall

References

[1] J. Kim, Review of nucleate pool boiling bubble heat transfer mechanisms, Int. J. Multiphase Flow, 2009, vol. 35 (12), pp. 1067-1076.

[2] V.K. Dhir, Mechanistic prediction of nucleate boiling heat transfer–Achievable or a hopeless task?, J. Heat Transfer., 2006, vol. 128 (1), pp. 1-12.

[3] M. Markels, R.L. Durfee, The effect of applied voltage on boiling heat transfer, AIChE J, 1964, vol. 10, pp. 106-110.

[4] M.M. Ohadi, N. Sharaf, D.A. Nelson, Electrohydrodynamic enhancement of heat transfer in a shell-and-tube heat exchanger, Exp. Therm. Flu. Sci., 1991, vol. 4 (1), pp. 19-39.

[5] J. Ogata, A. Yabe, Augmentation of boiling heat transfer by utilizing the EHD effect-EHD behaviour of boiling bubbles and heat transfer characteristics, Int. J. Heat Mass Transfer, 1993, vol. 36 (3), pp. 783-791.

[6] J.S. Cotton, A.J. Robinson, M. Shoukri, J.S. Chang, A two-phase flow pattern map for annular channels with and without a DC applied voltage and the application to electrohydrodynamic convective boiling analysis, Int. J. Heat Mass Transfer, 2005, vol. 48 (25-26), 5536-5579.

[7] Y. Hristov, D. Zhao, D.B.R. Kenning, K. Sefiane, T.G. Karayiannis, A study of nucleate boiling and critical heat flux with EHD enhancement, Heat Mass Transfer, 2009, vol. 45 (7), pp. 999-1017.

[8] Z. Liu, C. Herman, J. Kim, Heat transfer and bubble detachment in subcooled pool boiling from a downward-facing microheater array in a nonuniform electric field, Ann. N. Y. Acad. Sci., 2009, vol. 1161, pp. 182-191.

[9] W. Panofsky, M. Phillips, Classical Electricity and Magnetism, 2nd ed., Addison-Wesley, Publishing Co., Reading, Massachusetts, 1962.

[10] J.S. Chang, A. Watson, Electromagnetic hydrodynamics, IEEE Trans. Dielectric Elec. Insu., 1994, vol. 1 (5), pp. 871-895.

[11] A. Cattide, G.P. Celata, P. Di Marco, W. Grassi, Experimental study on bubble detachment under variable heat load and the action of electric field, Exp. Therm. Flu. Sci., 2008, vol. 40, pp. 485-496.

[12] W. Dong, R.Y. Li, H.L. Yu, Y.Y. Yan, An investigation of behaviours of a single bubble in a uniform electric field, Exp. Therm. Flu. Sci., 2006, vol. 30, pp. 579-586.

[13] F. Chen, Y. Peng, Y.Z. Song, M. Chen, EHD behavior of nitrogen bubbles in DC electric fields, Exp. Therm. Flu. Sci., 2007, vol. 32, pp. 174-181.

[14] Y.C. Kweon, M.H. Kim, Experimental study on nucleate boiling enhancement and bubble dynamic behavior in saturated pool boiling using a nonuiform dc electric field, Int. J. of Mult. Flow, 2000, vol. 26, pp. 135-368.

[15] Z. Liu, C. Herman, D. Mewes, Visualization of bubble detachment and coalescence under the influence of a nonuniform electric field, Exp. Them. Flu. Sci., 2006, vol. 31, pp. 151-163.

[16] Y.Q. Zu, Y.Y. Yan, A numerical investigation of electrohydrodynamics (EHD) effects on bubble deformation under pseudo-nucleate boiling conditions, Int. J. Heat Fluid Flow, 2009, vol. 30 (4), pp. 761-767.

[17] H.B. Zhang, Y.Y. Yan, Y.Q. Zu, Numerical modelling of EHD effects on heat transfer and bubble shapes of nucleate boiling, Applied Math. Model., 2010, vol. 34 (3), pp. 626-638.

[18] R. Kempers, P. Kolodner, A. Lyons, A.J. Robinson, A high-precision apparatus for the characterization of thermal interface materials, Rev. Sci. Instrum., 2009, vol. 80, 095111.

[19] S. Siedel, S. Cioulachtjian , J. Bonjour, Experimental analysis of bubble growth, departure and interactions during pool boiling on artificial nucleation sites, Exp. Therm. Fluid Sci., vol. 32, Issue8, pp. 1504-1511, 2008.

[20] A.J. Robinson, R.L. Judd, The dynamics of spherical bubble growth, Int. J. Heat Mass Transfer, 2004, vol. 47 (23), pp. 5101-5113.

[21] L.Z. Zeng, J.F. Klausner, R. Mei, A unified model for the prediction of bubble detachment diameters in boiling systems, 1993, Int. J. Heat Mass Trans., vol. 36, pp. 2261-2270.

[22] H.C. Lee, B.D. Oh, S.W. Bae, M.H. Kim, J.Y. Lee, I.S. Song, Partial nucleate boiling on the microscale heater maintaining constant wall temperature, Int. J. Multiphase Flow, 2003, vol. 29 (12), pp. 1857-1874.

[23] M. Jenny, J. Dušek, G. Bouchet, Instabilities and transition of a sphere falling or ascending freely in a newtonian fluid, J. Fluid Mech., 2004, vol. 508, pp. 201-239.

[24] F.N. Peebles, H.J. Garber, Studies on the Motion of Gas Bubbles in Liquids, Chem. Eng. Progress, 1953, vol. 49, pp. 88-97.

Appendix: Bubble forces at departure

An analysis on the forces governing bubble detachment has been performed. Based on the analysis described in Zeng et al. [21], the forces to be considered are the surface tension force, the unsteady growth force, the buoyancy force, the contact pressure force and the lift force. Assuming quasi-static growth, the sum of all the vertical forces is close to zero while the bubble remains attached to the surface. The surface tension force is somewhat difficult to estimate due to the fact that the bubbles always stay attached to the nucleation site. The contact angle at the triple interface is thus not well defined as it could be located slightly below the plane of the surface within the cavity where there is no visual access. The buoyancy and contact pressure forces, as well as the unsteady growth force can, however, be estimated. Consistent with the analysis of Zeng et al. [21], the lift force is considered to be negligible.

In the following analysis a bubble close to detachment is considered for the highest Jakob number experiments and the Zeng et al. formulation of the forces is implemented.

The buoyancy force can be expressed as:

$$F_{buy} = V(\rho_l - \rho_v)g \tag{1}$$

where V is the bubble volume, ρ represents the densities of liquid and vapour and g is gravitational acceleration. For a bubble close to detachment: $F_{buy} \cong 3 \times 10^{-6}\ N$.

The contact pressure force can be expressed as:

$$F_{cp} = \frac{\pi d_w^2}{4}\frac{2\sigma}{r_r} \tag{2}$$

where d_w is the vapour bubble contact diameter, σ is the surface tension and r_r the radius of curvature at the base of the bubble. The value of $2\sigma/r_r$ is the pressure difference between the liquid and the vapour. A first estimation of the static pressure difference can be obtained using the bubble radius as the curvature for r_r such that $F_{cp} \cong 1.6 \times 10^{-6}\ N$.

The Zeng et al. model of the unsteady growth force is predicted by:

$$F_{ug} = -\rho_l \pi a^2 \left(\frac{3}{2}C_s\dot{R}^2 + R\ddot{R}\right) \tag{3}$$

where R is the bubble radius and $\dot{R}$ and $\ddot{R}$ are the interface velocity and acceleration respectively. Here, C_s is an empirical constant given as $C_s = 20/3$. For situations in which the vapor bubble growth approximately obeys a power law, $R(t) = Kt^n$, the inertial force can be expressed as:

$$F_{ug} = -\rho_l \pi K^{\frac{2}{n}} \left[\frac{3}{2} C_s n^2 + n(n-1)\right] R^{4-\left(\frac{2}{n}\right)} \quad (4)$$

As was discussed, the present measurements are such that $R(t) = \left(\frac{3V_d}{4\pi t_d}\right)^{\frac{1}{3}} \times t^{0.2}$ with V_d and t_d being the bubble volume and time at detachment. Taking the maximum Jacob number case, i.e. the fastest bubble growth, $V_d = 0.5 \times 10^{-9}\ m^3$ and $t_d = 0.07\ s$. This gives $F_{ug} \cong -2.4 \times 10^{-8}\ N$ which is two orders of magnitude lower than the buoyancy force. This is due to the fact that the experiments were performed at relatively low Jakob numbers combined with the fact that bubble growth is generally asymptotic, such that is typically slow near detachment.

As the bubble has not yet fully detached, the sum of all vertical forces acting on the bubble should be close to zero. This being the case, the sum of the buoyancy and contact pressure forces must be balanced by the surface tension force. In this way an estimation of the contact angle can be made using the following expression of the surface tension forces at the triple contact line:

$$F_\sigma = -\pi d_w \sigma \sin\Gamma$$

Balancing this force with the sum of the buoyancy and contact pressure forces, the contact angle is found to be $\Gamma \approx 34°$. Such a low dynamic contact angle, indicating a wetting liquid, is consistent with the measured static contact angle of sessile drops of pentane on polished copper which was approximately 5°.

Figure captions:

Figure 1: Schematic of the experimental setup

Figure 2: Schematic of the test sample

Figure 3: Geometry of the nucleation site observed with a white light confocal microscope

Figure 4: Image processing samples

Figure 5: Single phase convection above the experimental sample for a wall superheat of θ_w=30 K (a) V_0 = 0 kV, (b) V_0 = 24 kV.

Figure 6: Single phase heat transfer enhancement. The plain and dashed lines are respectively the 0 kV and the 24 kV regression fits.

Figure 7: Bubble growth sequence for (a) V_0 = 0 kV and (b) V_0 = 24 kV. Elapsed time between two successive frames is about 5.7 ms.

Figure 8: Normalized bubble growth for various wall superheats without an electric field.

Figure 9: Normalized bubble growth for various wall superheats with an electric field at 24 kV.

Figure 10: Rate of change of normalized bubble volume with and without an electric field.

Figure 11: Photographic sequence of bubble rise for the case of no electric field.

Figure 12: Height of the free bubble centre of gravity versus time subsequent to departure.

Figure 13: Bubble vertical velocity and displacement from the central vertical axis of the cavity.

Figure 14: Maximum vertical velocity of the bubbles in the presence of an electric field

Figure1

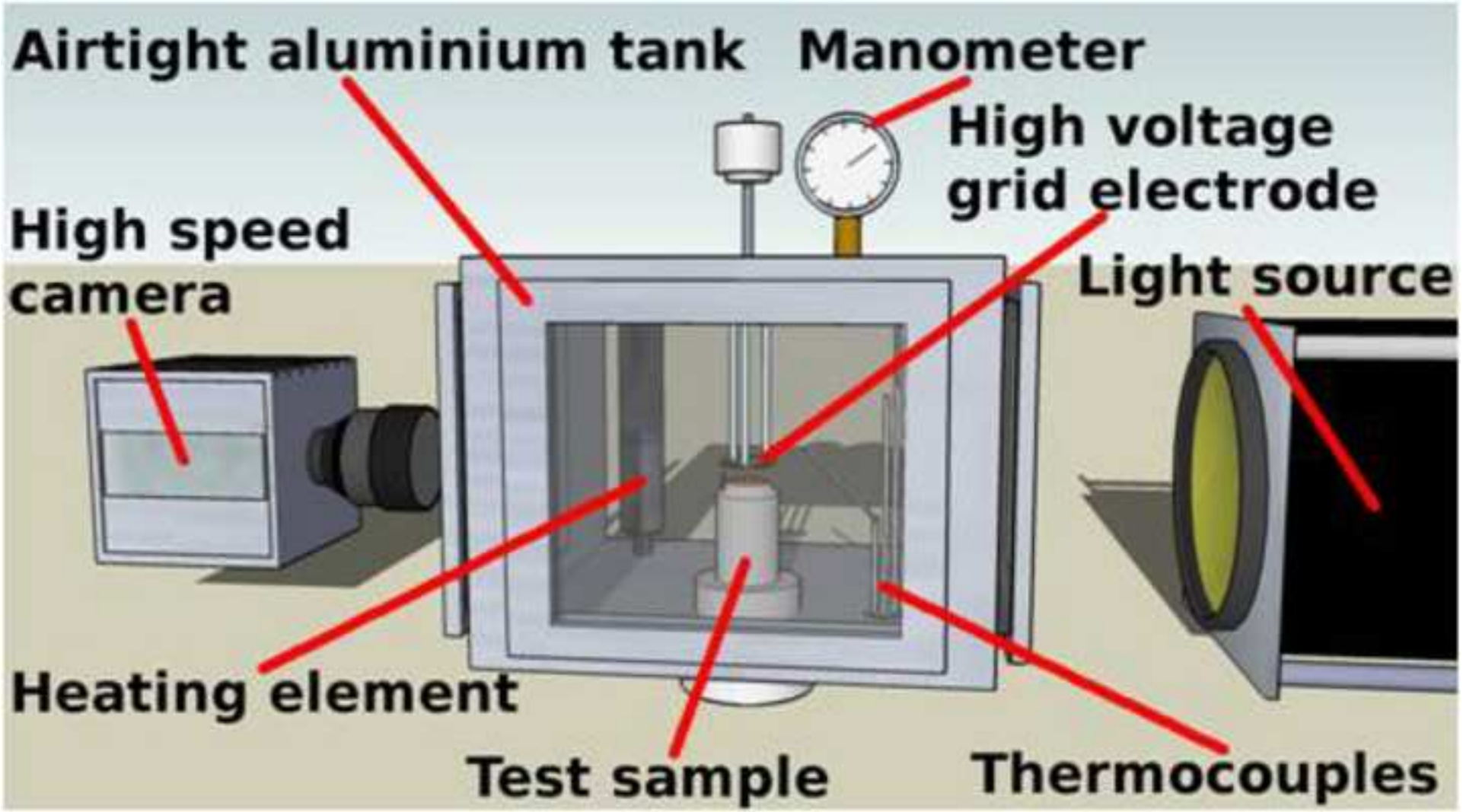

Figure2

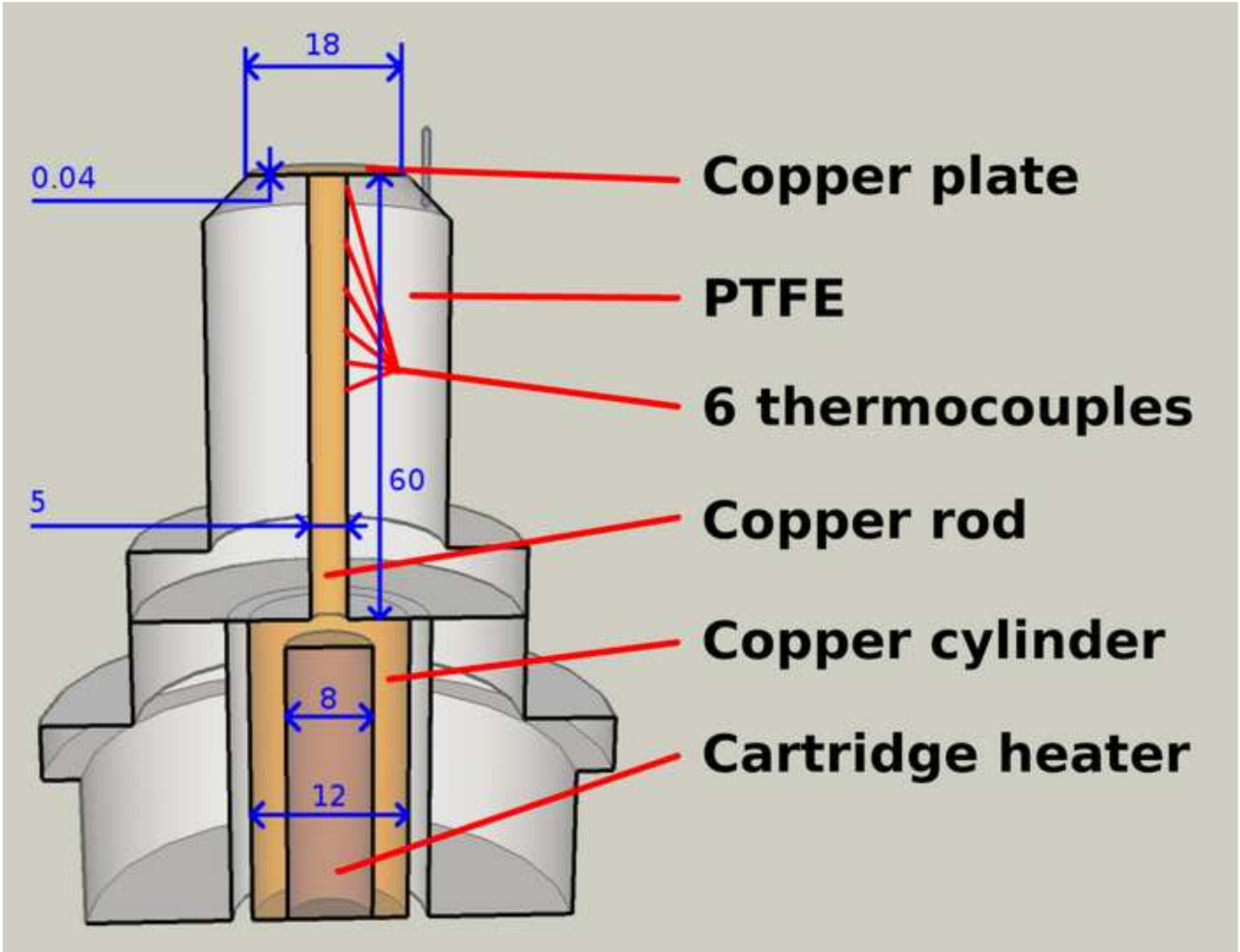

Figure3

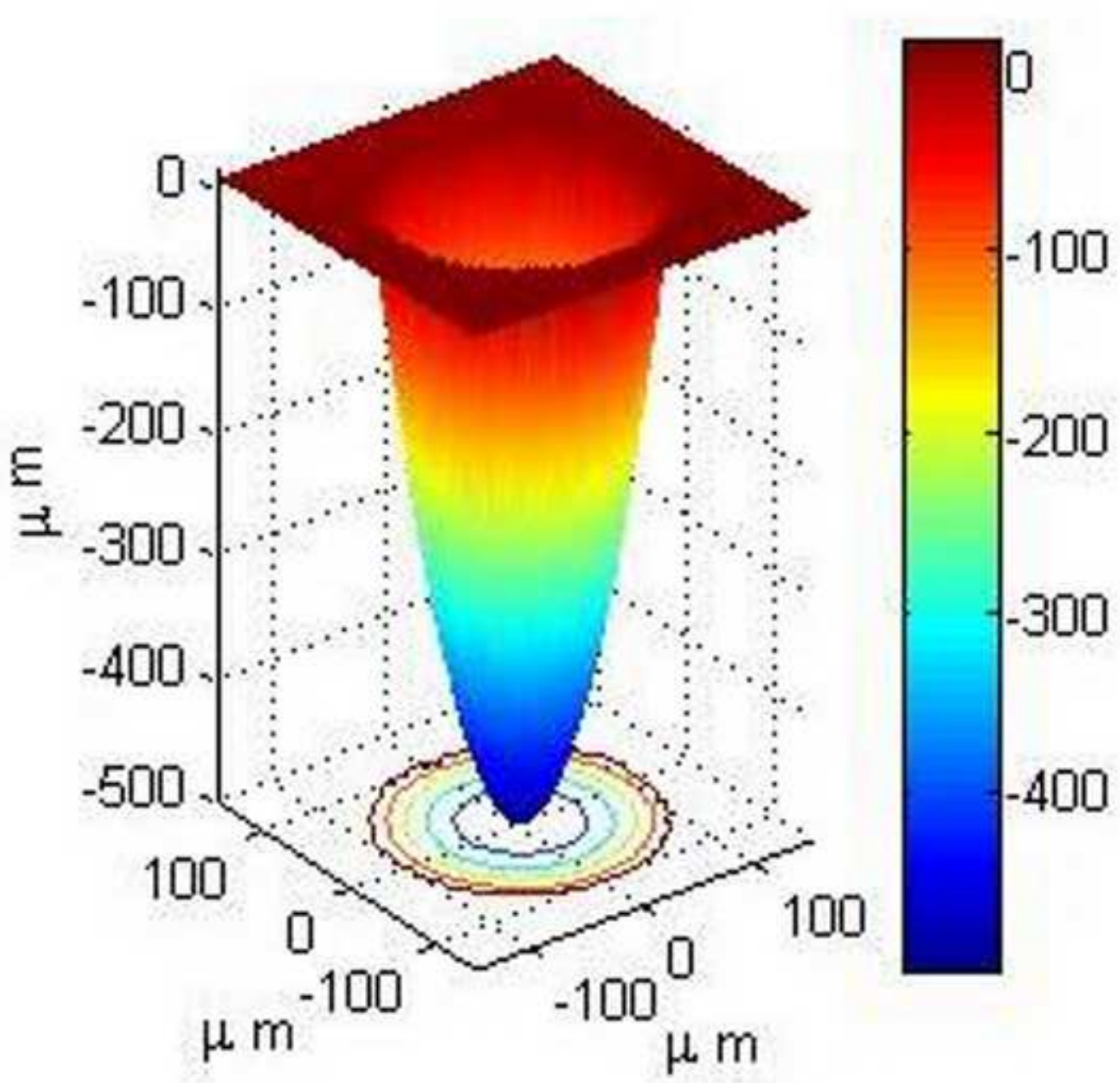

Figure4

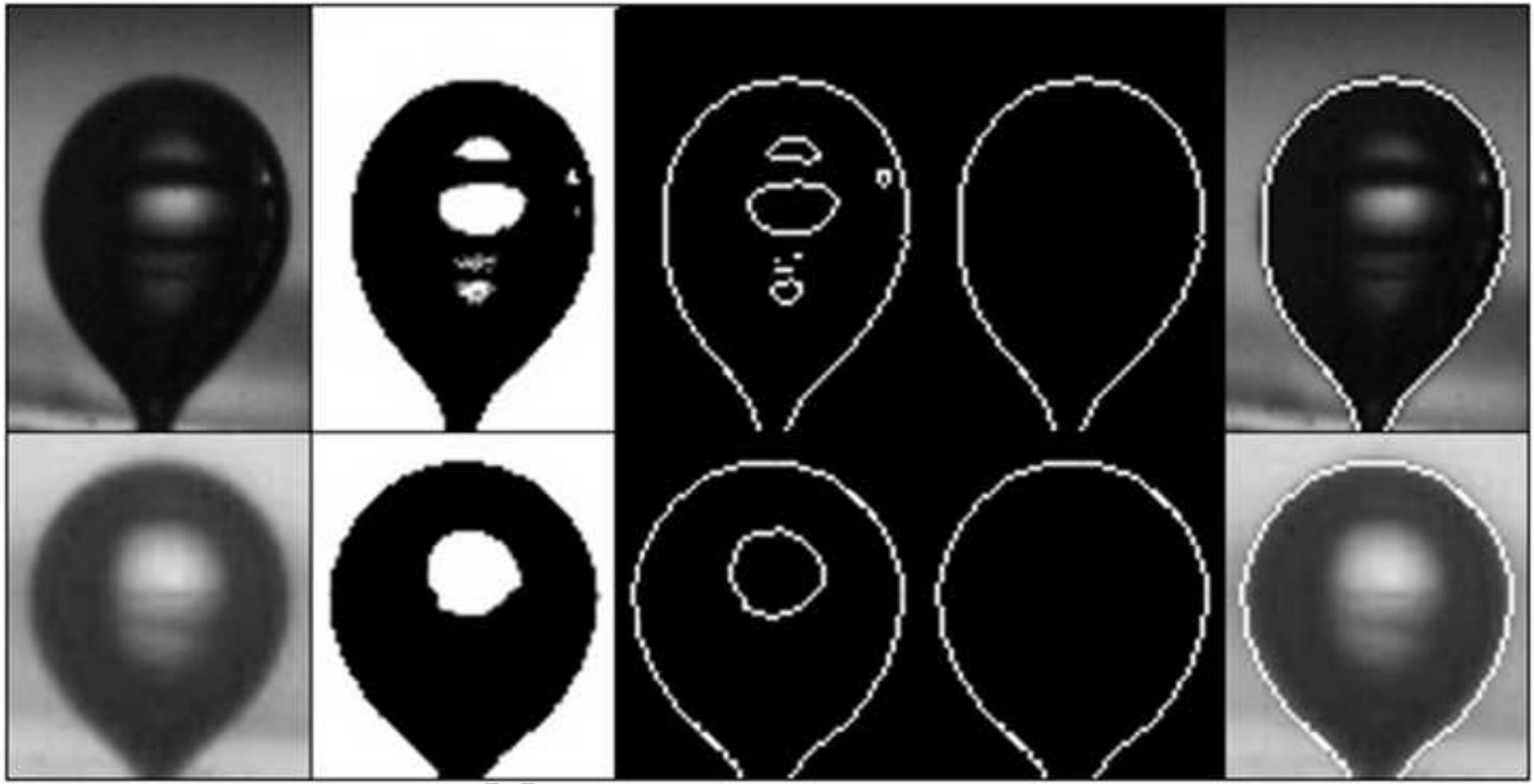

Figure5

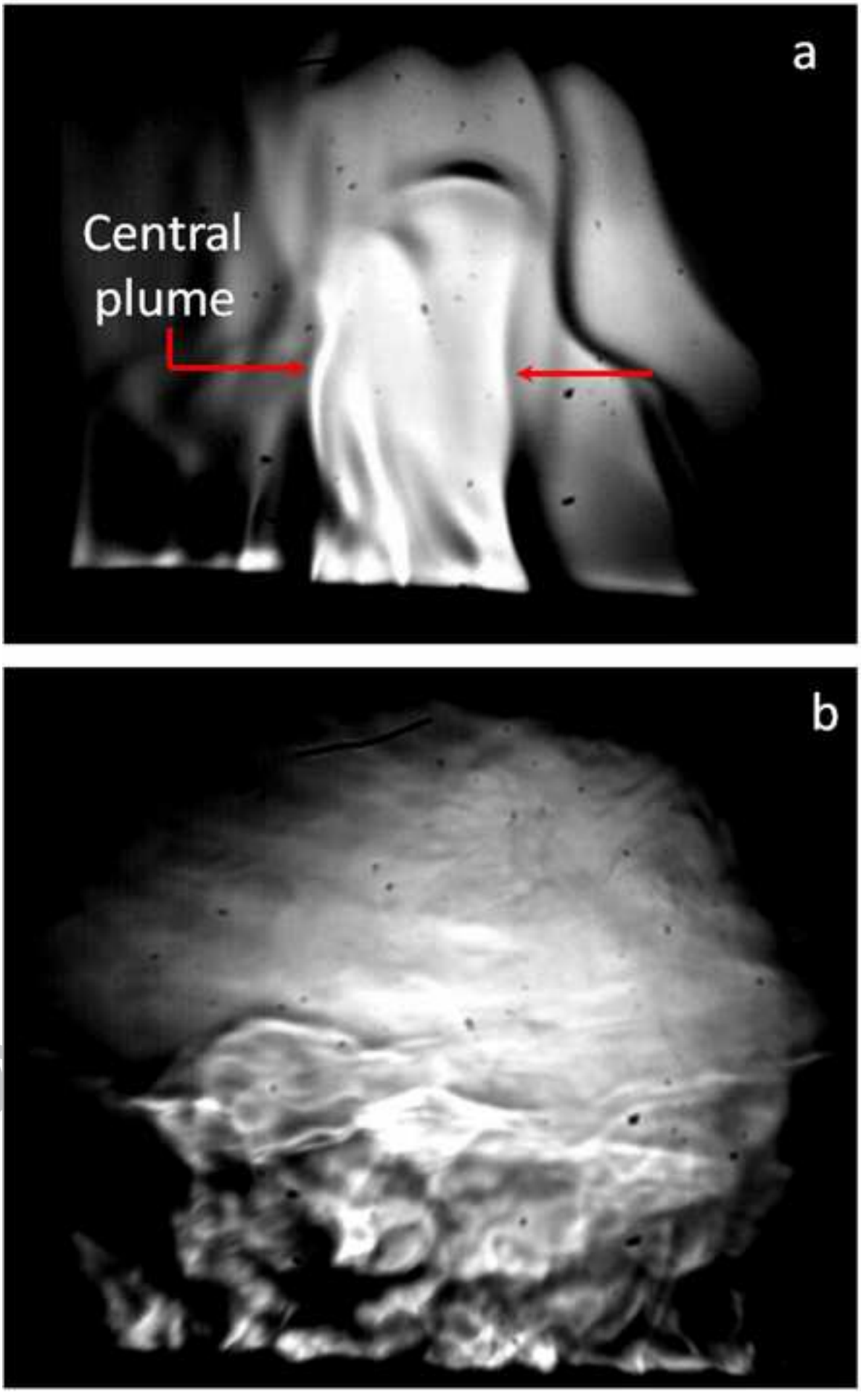

Figure6

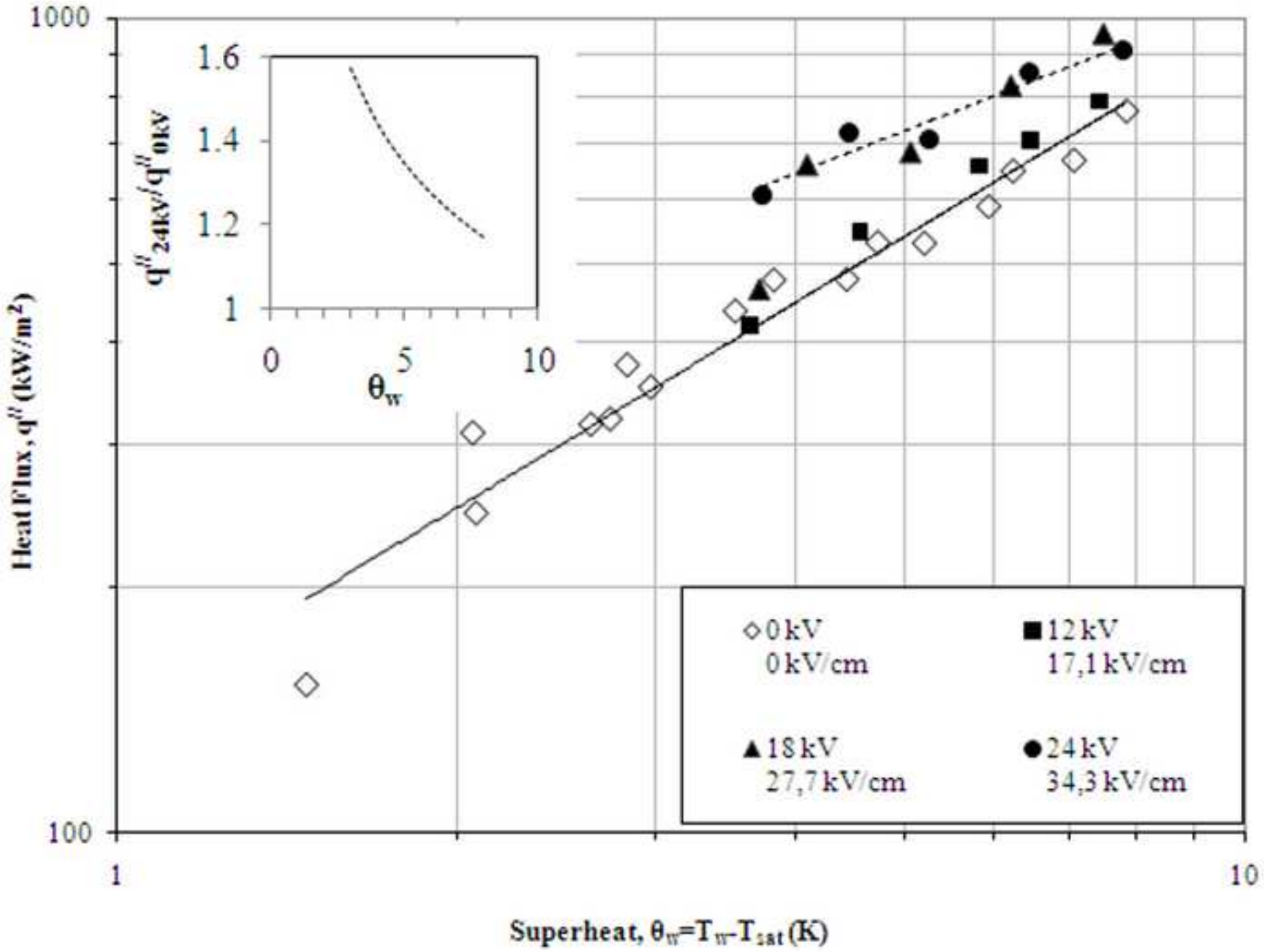

Figure7

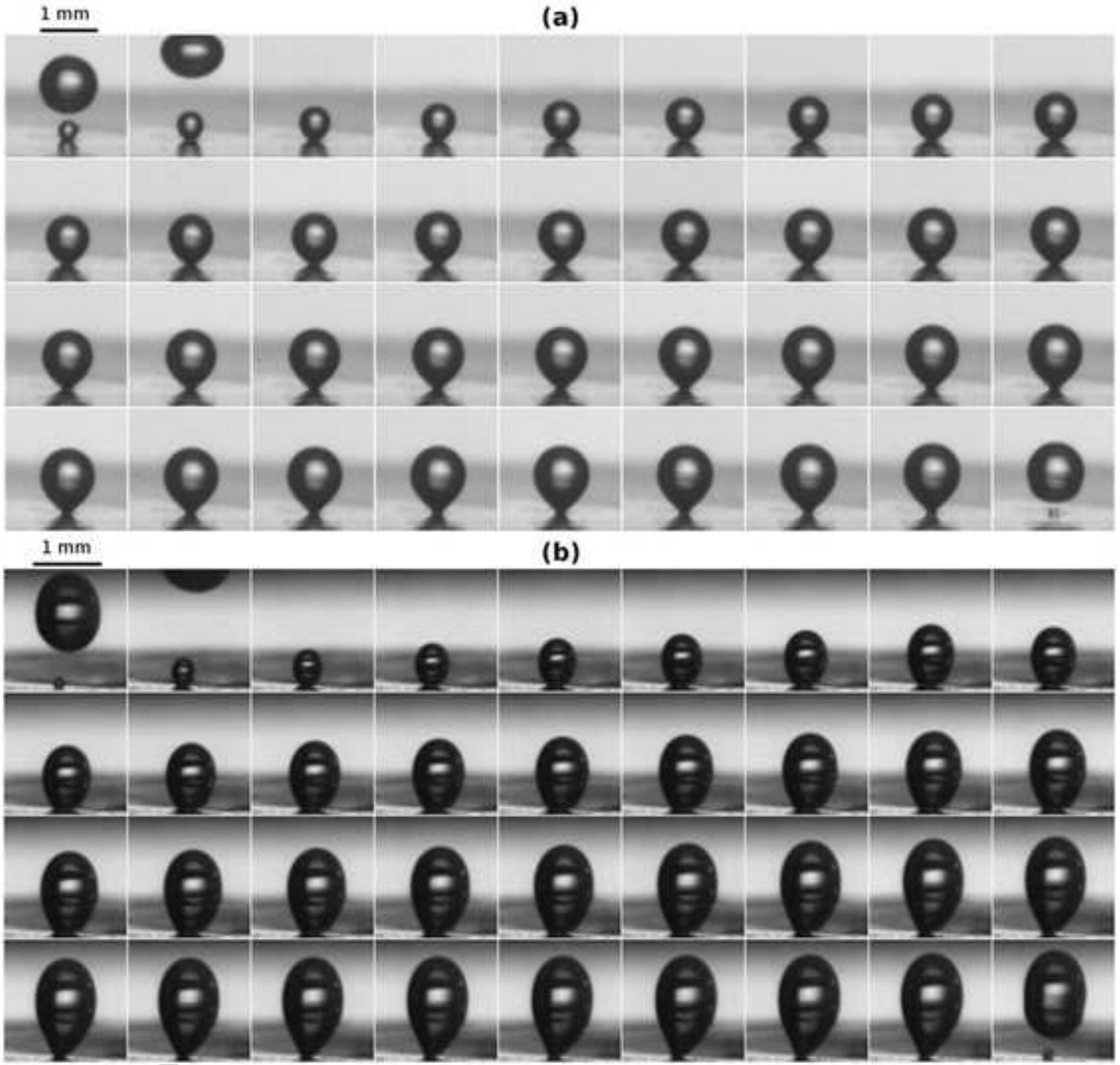

Figure8

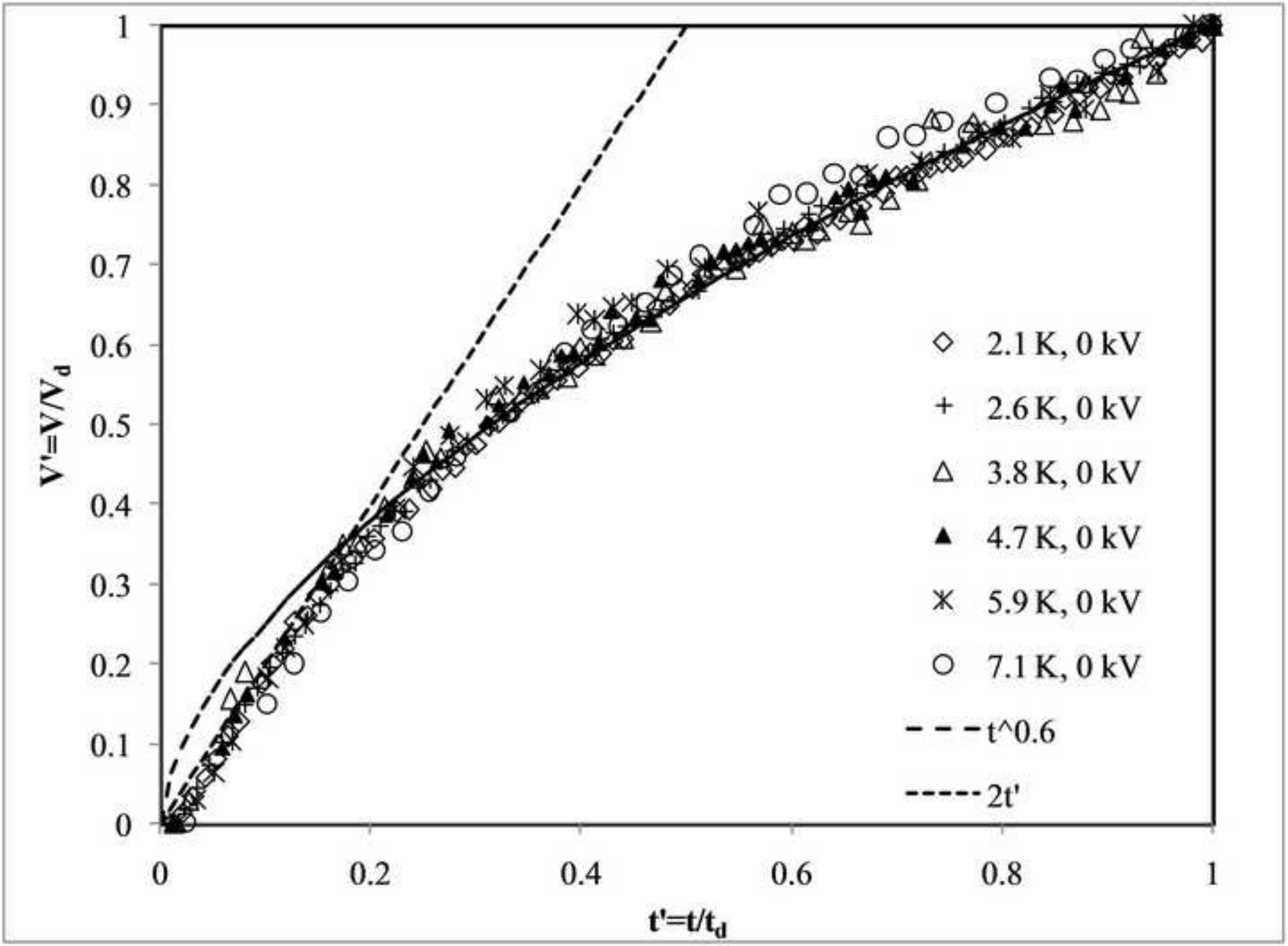

Figure9

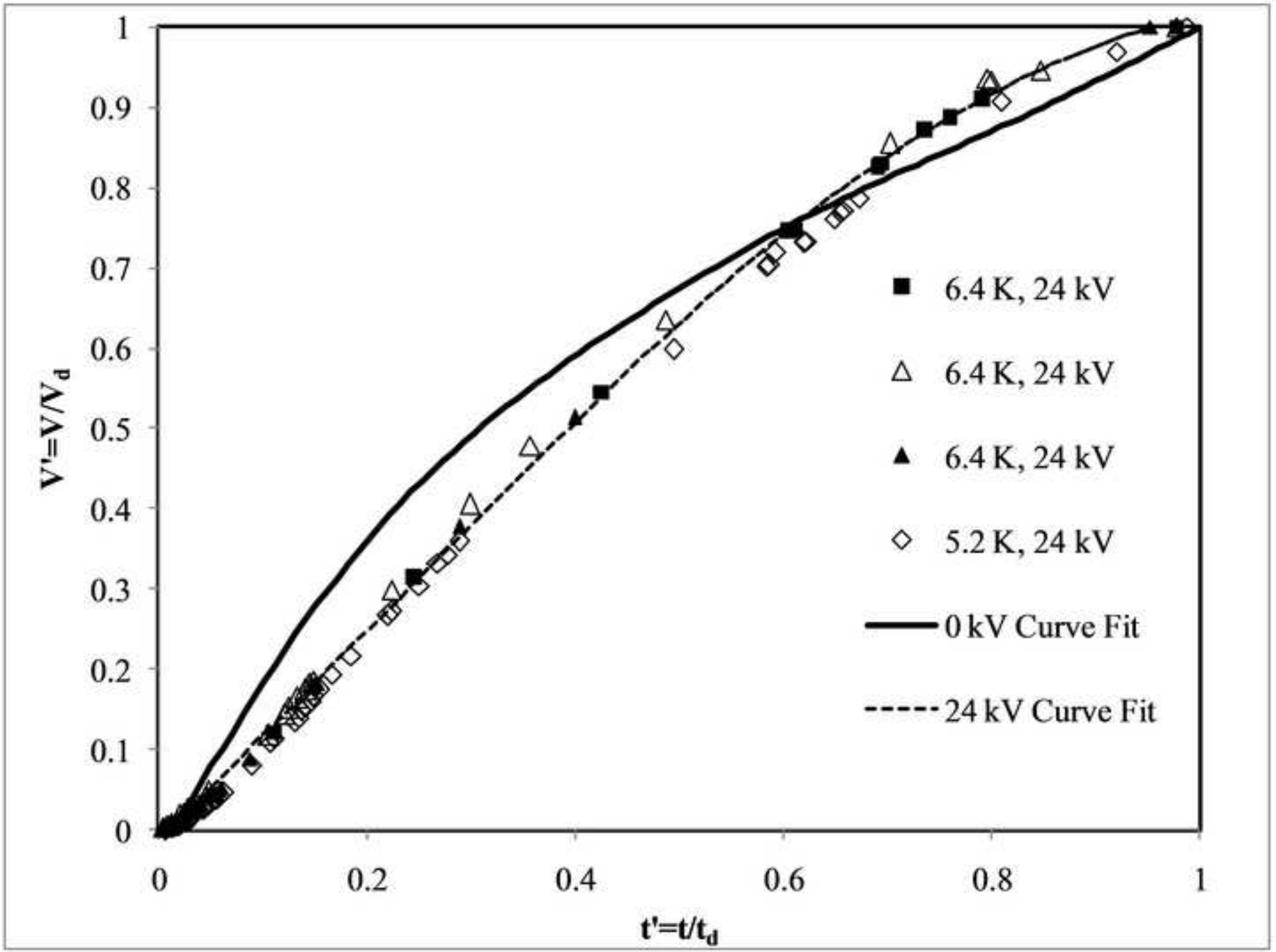

Figure10

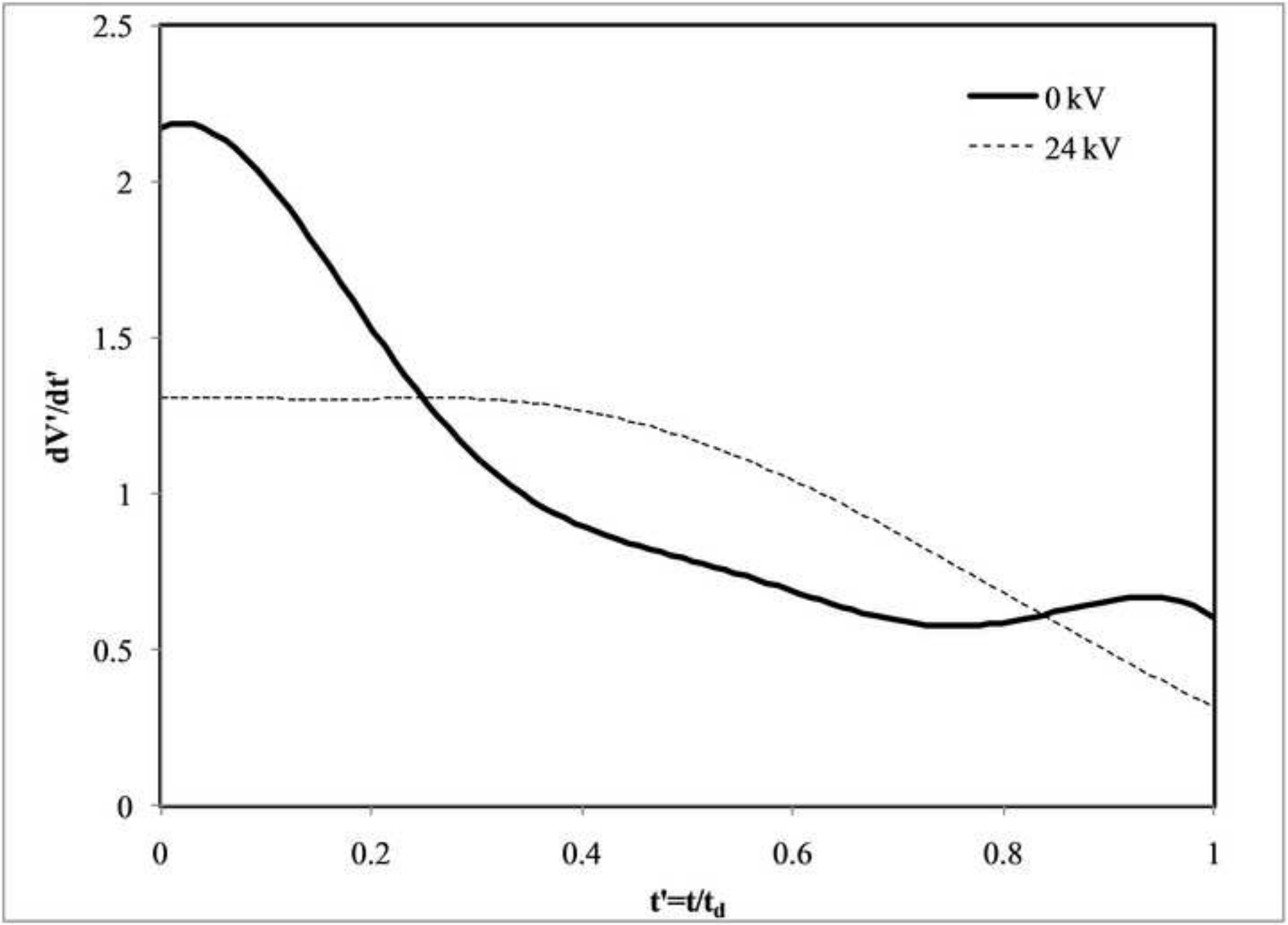

Figure11

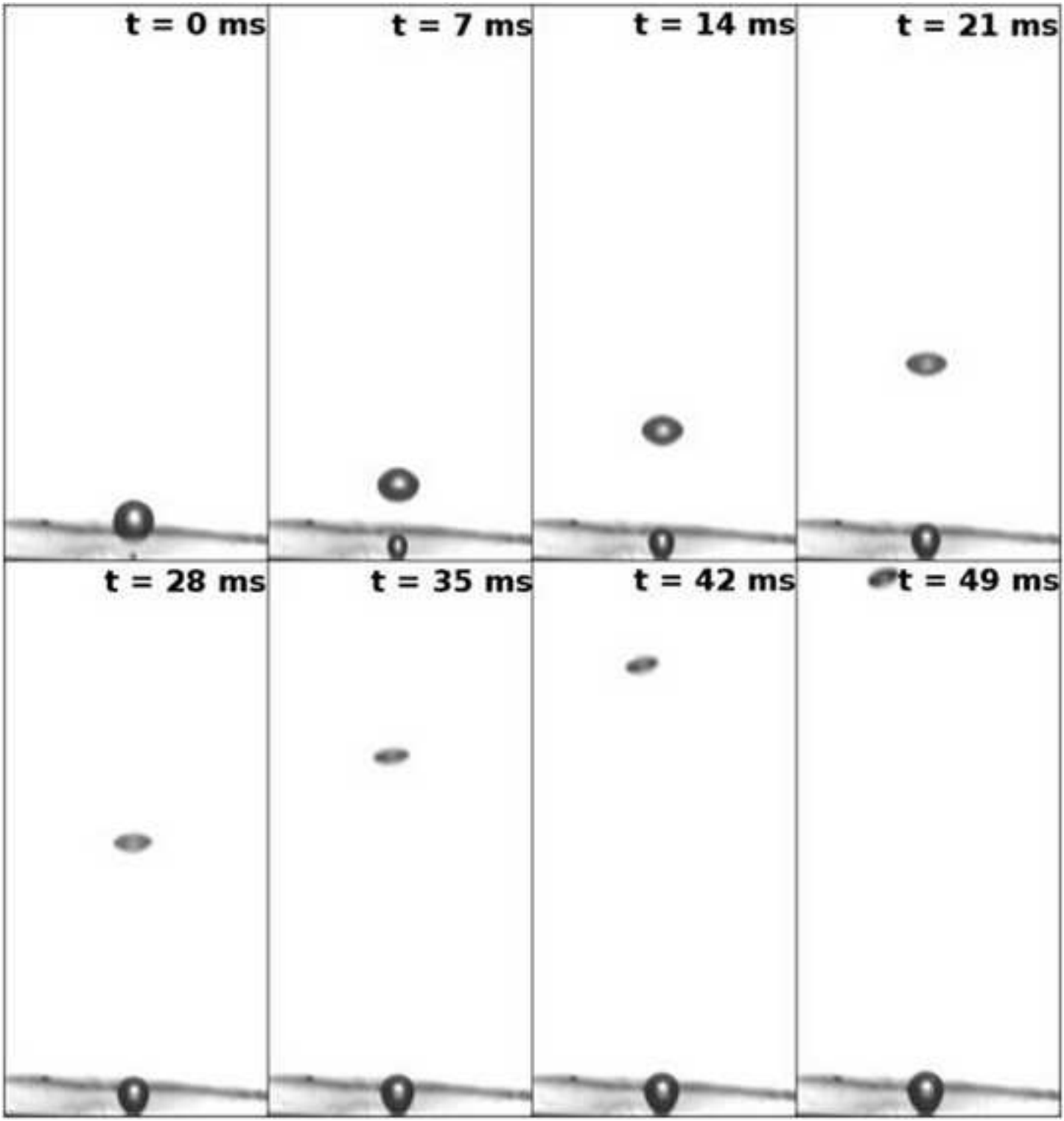

Figure12

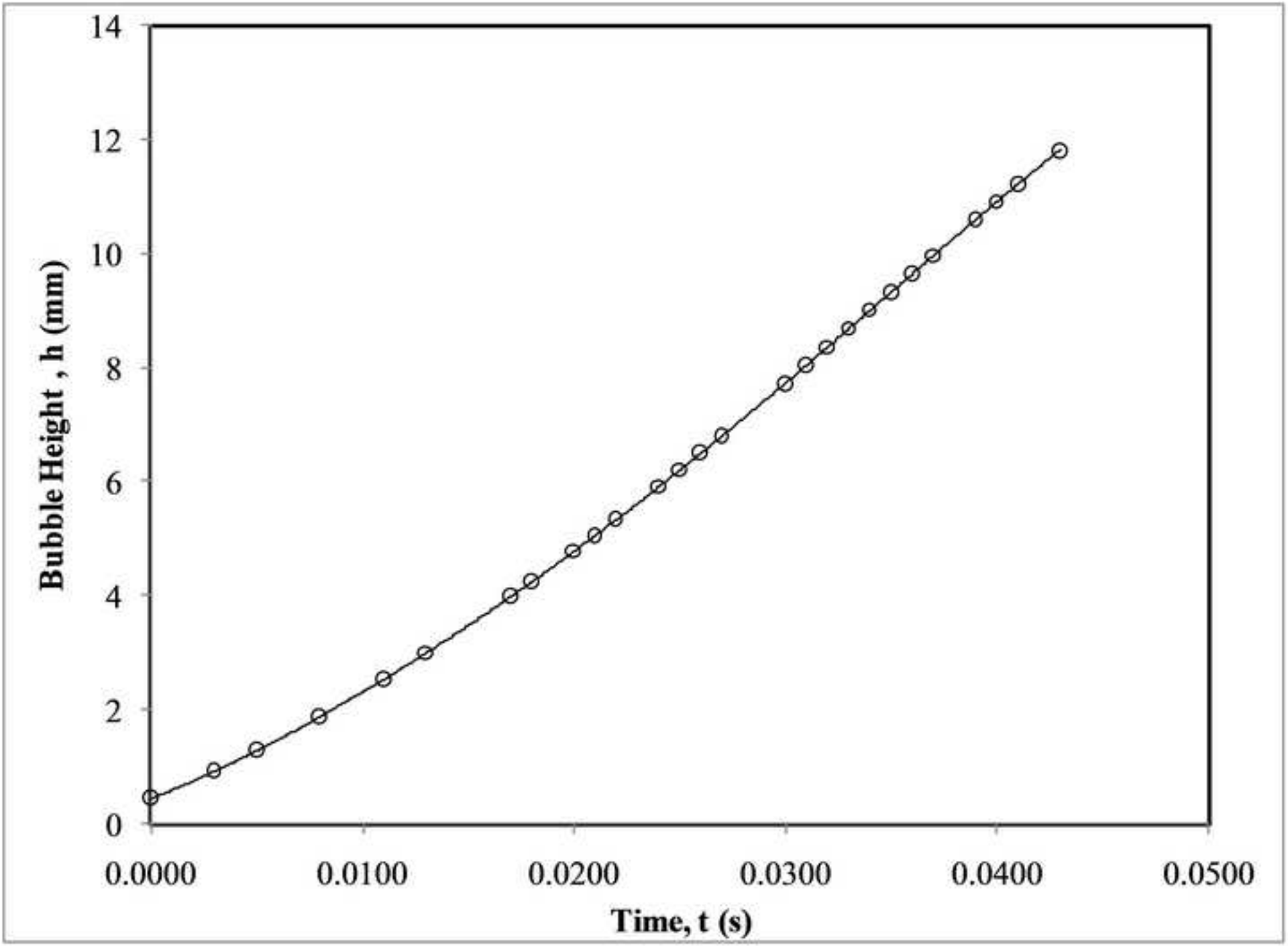

Figure13

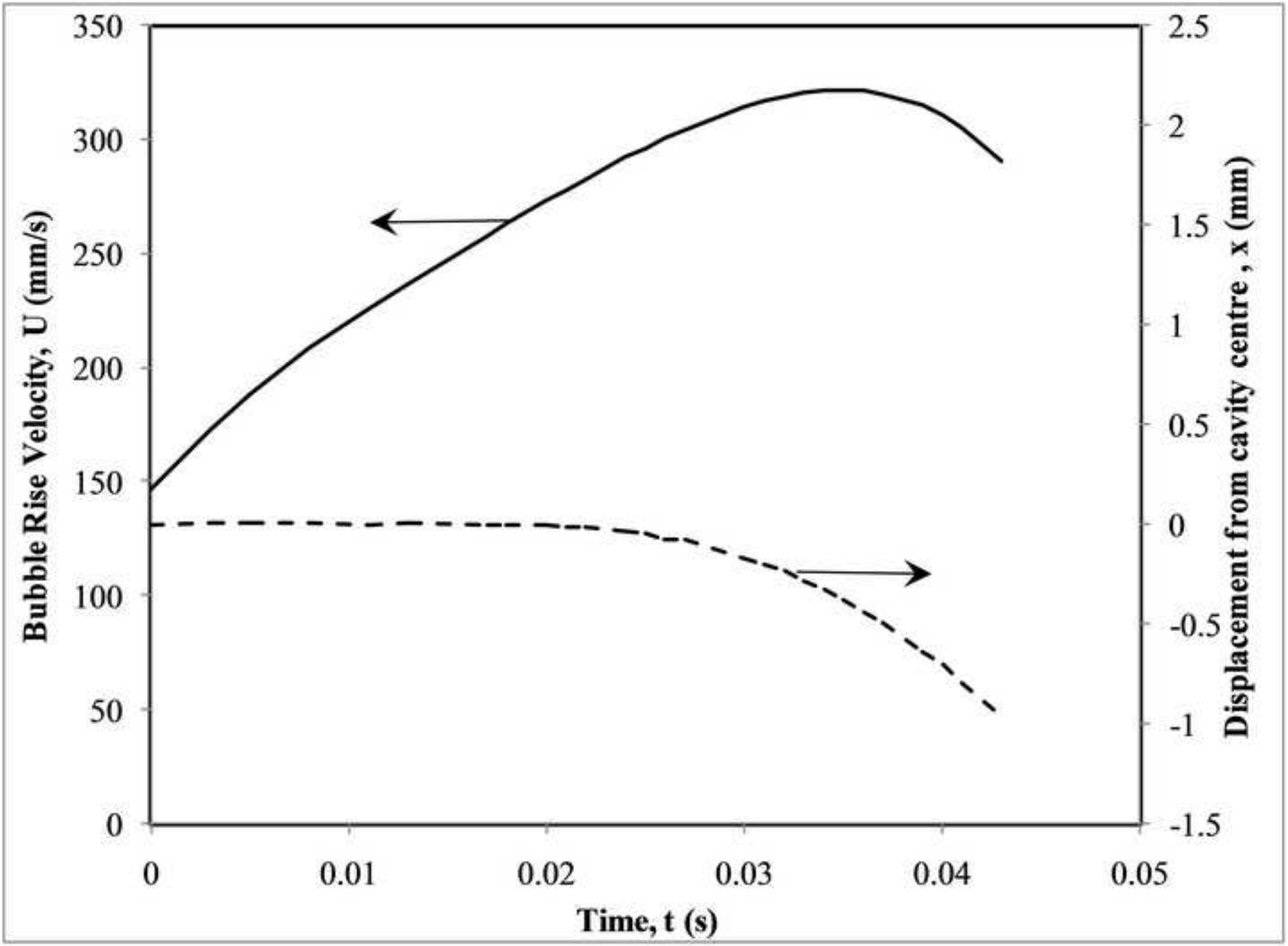

Figure14